Thermal Influence on the Stiffness of Hybrid Metal-Composite Countersunk Bolted Joints

Calin-Dumitru COMAN*

*Corresponding author
INCAS – National Institute for Aerospace Research "Elie Carafoli",
B-dul Iuliu Maniu 220, Bucharest 061126, Romania,
coman.calin@incas.ro

Abstract: *This paper presents the effects of temperature on the axial stiffness of a hybrid metal-composite countersunk bolted joint designed for the bearing failure mode. A detailed 3D finite element model incorporating geometric, material and friction-based full contact nonlinearities is developed to numerically investigate the temperature effects on joint stiffness. In order to validate the temperature effects, experiments were conducted using an Instron testing machine coupled to a temperature controlled chamber. The results showed that the temperature effects on axial joint stiffness were quite accurately predicted by the 3D finite element model, denoting a reduction in the stiffness of the axial joint with an increase in temperature for hybrid metal-composite countersunk bolted joints.*

Key Words: *Hybrid bolted joints, finite element analysis, temperature, joint stiffness*

1. INTRODUCTION

The aerospace industry became the most common application field for fiber-reinforced polymer matrix composites (PMCs) due to their lightweight properties [1]. These structural components are often assembled in conjunction with metal parts using mechanically fastened joints resulting in hybrid metal-composite joints which generate some challenging problems for mechanical engineers. Poorly designed hybrid joints are not only a source of failure, but could lead to a reduction of the durability and reliability of the whole structure. Up to nowadays, the researchers studied the failure analysis of composite bolted joints using a method that combines continuum damage mechanics (CDM) [2] with finite element analysis (FEA). In the CDM case, the local damage onset appears at low values of the applied load and damage accumulation is developed with increasing load according to damage propagation laws, which makes the method accurate and able to predict various failure modes. The major disadvantage of the CDM models is the huge amount of test data required for model calibrations. The progressive damage analysis (PDA) of composite materials, which is based on the stress-strain failure criterion [3], showed that the material orthotropic properties reduction due to damage initiation is essential for the stress field analysis [4-7]. Many PDA models [8-11] incorporated shear nonlinearity, the Hashin type failure criterion and constant elastic properties degradation laws for orthotropic materials, which make the method quite easy to implement and computationally efficient. Because these properties degradation models used constant factors for elastic properties reduction due to damage growth, the models

weren't able to predict the bearing final failure.

Models containing continuous degradation rules have begun to appear in the literature [12-13], in order to improve the numeric algorithm convergence and to obtain a smoother load-displacement curve. A major shortcoming of these models is that they focused on only a few types of failure modes and did not consider the different modes of joint failure. The composite progressive damage behavior is a complex nonlinear phenomenon and in conjunction with geometric and contact nonlinearities can lead to loss of convergence in the finite element method (FEM) analysis, mostly in implicit numerical algorithms that involve a lot of effort to obtain a solution for predicting the final failure of the global structure.

The composite materials can withstand an increased temperature up to 300^0C, having good properties as: high pressure resistance, low thermal expansion coefficient, high thermal conductivity, high thermal shock resistance and low depression [14]. The difficulties arising from composite materials usage on structural failure problems are that these materials have anisotropic mechanical properties, brittle behavior and low inter-laminar strength [15]. Another issue is the damage in composite materials variation with the temperature as described in [16-19]. Airplane structures can be exposed to rush environment conditions which can imply the joints strength loss because of environmental ageing and temperature variations, these topics being studied in the research community [20-25].

This study describes and develops a progressive damage analysis using an adequate material model for composite adherent that can predict the thermal effects on the structural behavior and the failure modes of the hybrid metal-composite bolted joints by taking into account all the nonlinearities phenomena involved in the load transfer trough the joint as geometric nonlinearity; this implies: large deformations, friction based full nonlinear contact and material nonlinearities due to the lamina shear deformations. The Hashin-type failure criterion and strain-based continuous degradation rules were implemented using a user subroutine in the commercial Nastran SOL 400 solver. A series of experiments were conducted to validate the FE model and PDA results, involving the influence of temperature on the failure modes of the hybrid-metal composite joints. The experimental and numerical results fit together quite accurately capturing the influence of temperature on the stiffness and failure load of the hybrid metal-composite bolted joints.

2. PROBLEM DESCRIPTION

- Joint geometry description

Single-lap joints (SLJ) with countersunk bolts were manufactured using both metal and composite materials for the adherents. The geometry of the joint model is presented in Fig. 1. The joint design was chosen in accordance with ASTM D 5961 standard, [26], to induce bearing failure. The dimensions each adherent are the same, as follows: 150 mm length and 50 mm width, but the thicknesses are different, the metal adherent has 4 mm thickness and the laminated adherent has 2 mm; a similar geometry was previously used in [27]. Countersunk head stainless steel bolts with nominal diameter of 4 mm and a 0.5 Nm torque level were used in dry conditions. The composite adherent was manufactured from carbon-epoxy pre-pregs with 32% fiber volume fraction. The stacking sequence of the composite adherent is represented by [0/90/0/90/0/90] using 0.33 mm thickness unidirectional lamina, with the elastic properties presented in Table 1. The metal adherent was manufactured from aluminum alloy AA 7075T6 and the bolts, nuts and washers were fabricated from stainless steel A2-70 with the elastic properties, also presented in Table 1. A group of five SLJs were prepared for

the thermal effects study on the failure mechanisms in the laminated adherent.

Regarding the clamping of the joint in the testing machine, the boundary conditions imposed on the FE model are presented in Fig. 1. The displacements *u*, *v* and *w* are defined in x, y and z directions.

The boundary conditions represent clamping the nodes on top and bottom surfaces at the leftmost end of the metal adherent and blocking the translations on y and z directions (*v* and *w*) at the rightmost end of the composite adherent.

For simulating the quasi-static loading condition of the testing machine, a prescribed displacement, on x direction (*u*) is used for the nodes from both surfaces of the composite adherent at the rightmost end.

The dimensions of the joint geometry are designed in such a way that allow the bearing failure in the laminated composite adherent and are explained in Fig. 2.

The mechanical properties of the materials used are presented in Tables 1 and 2, where the lamina orthotropic directions (1, 2, 3) are the same with global coordinate axes (x, y, z) shown in Fig. 1.

The lamina elastic properties presented in Table 1 were obtained using ASTM [28-30] standard tests on the unidirectional laminated specimens. Regarding the thermal expansion coefficient of the composite adherent, a micro-analysis method was used to calculate this coefficient at lamina level, using the thermal coefficients of the fibers and matrix. According to [31-32] we have $\alpha_{fiber} = -0.41 \cdot 10^{-6}/$ °C, $\alpha_{matrix} = 40 \cdot 10^{-6}/$ °C. Using these values and equation (1) it can be obtained [3]:

$$\alpha_{11} = \frac{E_{fiber} \cdot V_{fiber} \cdot \alpha_{fiber} + E_{matrix} \cdot (1 - V_{fiber}) \cdot \alpha_{matrix}}{E_{11}} = 2 \cdot 10^{-6}/°C \qquad (1)$$

$$\alpha_{22} = \alpha_{33} = 44 \cdot 10^{-6}/°C \qquad (2)$$
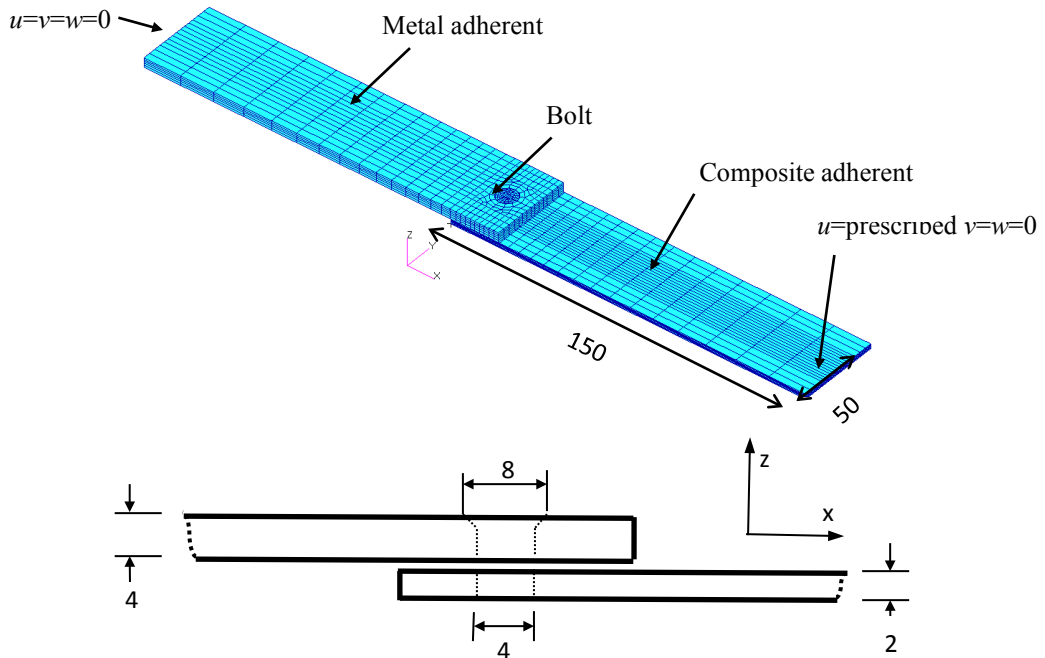
Figure 1. Countersunk joint geometry and boundary conditions, all dimensions (mm)
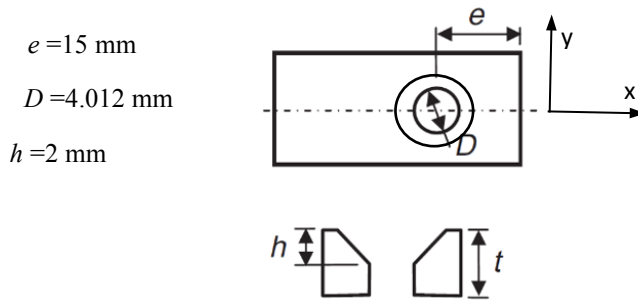
e =15 mm

D =4.012 mm

h =2 mm

Figure 2. Specimen dimensions for bearing failure mode, [27]

Table 1. Composite Material Properties

Property	Carbon fibers [31]	Epoxy matrix [32]	Lamina EXP.
Longitudinal modulus E_{11} (MPa)	230000		34433
Transversal modulus E_{22} (MPa)	6000	3200	3610
Through-thickness modulus, E_{33} (MPa)		3200	3610
Shear modulus G_{12} (MPa)	18000	1300	2421
Shear modulus G_{23} (MPa)		1300	2421
Shear modulus G_{13} (MPa)		1300	1561
Poisson coefficient v_{12}	0.36	0.35	0.36
Poisson coefficient v_{23}		0.35	0.45
Poisson coefficient v_{13}		0.35	0.35
Longitudinal CTE α (10^{-6}/^{o}C)	-0.04	4	2
Transversal CTE α (10^{-6}/^{o}C)			44
Through-thickness CTE α (10^{-6}/^{o}C)			44
Longitudinal tensile strength $\sigma_{11, max}^T$, (MPa)	3530	86	253
Longitudinal compression strength $\sigma_{11, max}^C$, (MPa)			230
Transversal compression strength $\sigma_{22, max}^C$, (MPa)			74
In plane shear strength τ_{12}^{max}, (MPa)			25
Out plane shear strength τ_{23}^{max}, (MPa)			37
Out plane shear strength τ_{13}^{max}, (MPa)			37

Table 2. Isotropic Material Properties

Property	AA 7075T6 [34]	A2-70 [34]
Elastic modulus E (MPa)	71016	206000
Shear modulus G (MPa)	26890	75842
Poisson coefficient v	0.33	0.36
Thermal coefficient CTE α (10^{-6}/^{o}C)	24	18

After joint mounting, the specimen was gripped in the 30 kN Instron 3367 testing machine, connected to a temperature controlled chamber, Fig. 3.

The chamber is Instron SFL 3119-400, temperature controlled (-70/+250°C) with liquid CO_2 as freezing agent.

The bearing tests were conducted in accordance with ASTM 5961 standard, [26], and the specimens were loaded with a displacement rate of 0.3 mm/min until ultimate failure for the temperature values, T_1= +50°C, T_2= -50°C.
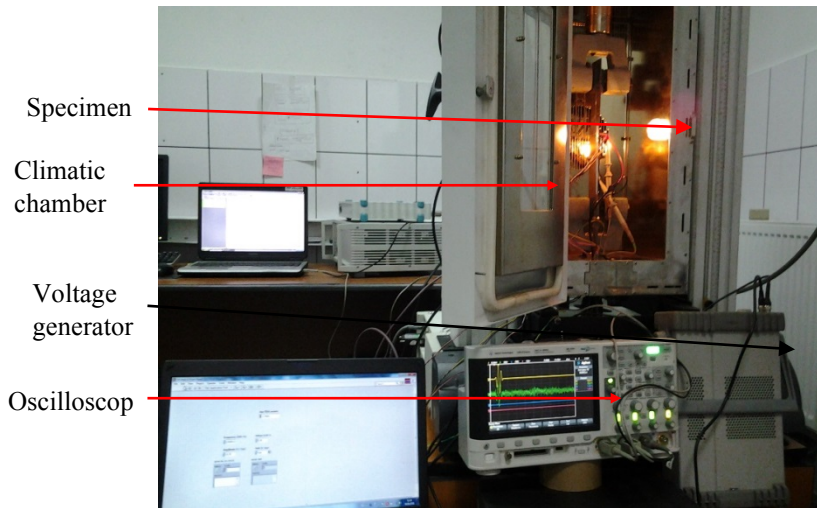
Figure 3. Experimental workbench

- Numerical model description

A tridimensional (3D) FEM, using linear brick elements with eight nodes was developed in the commercial software MSC Patran for the joint geometry model, as shown in Fig. 4. Each separate part was modeled: metal and composite adherents, the washer and a combined bolt-nut part. The adherents were modeled with increased radial mesh density around the hole, where high strain gradients exists. In order to avoid rigid body motions, light springs were attached to the components not fully constrained, such as the bolt, washer and laminated adherent. For simulating the bolt pre-load due to the applied torque level, a 330 N axial force was applied in the bolt shank using Bolt Preload Module in Patran.
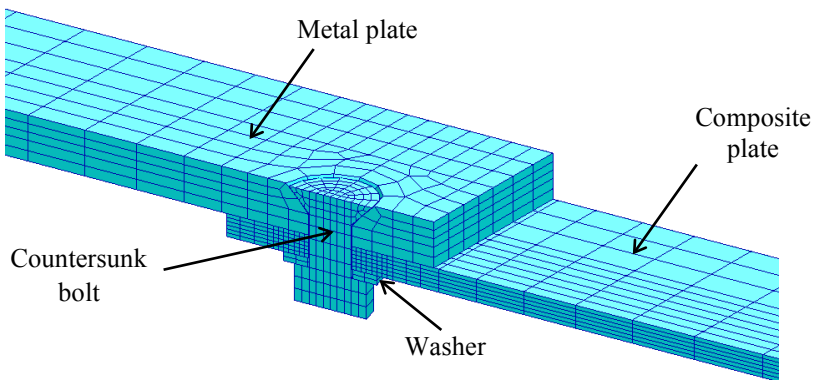

Figure 4. 3D finite element model

    The laminated adherent is modelled with continuum solid-shell special elements available in MSC Nastran 2012. These special solid elements have bending properties like shells and one integrating point per element is considered. The finite element model has six elements across the laminate thickness, with one solid-shell element per each ply, thus, stress in each ply can be determined and the correct bending-twisting coupling is obtained. The dimension for each part of the FE model is described in Table 3. The FE model was refined in the vicinity of the hole, due to the stress concentrators. Thus the minimum element length is 0.33 mm around the hole. The minimum element length is increasing from hole towards the clamped ends of the adherents. In the 3D model, the contact with clearance between the bolt and the

surface of the hole is realized as follows. The method requires the definition of the bodies that can come into contact. The contact bodies may be the whole physical bodies (laminated adherents, bolt, washer), but it has been shown in [35] that it is more efficient to consider sets of elements of these physical bodies, as shown in Fig. 5, because the number of checks for the contact between bodies at each iteration of the solution is reduced.
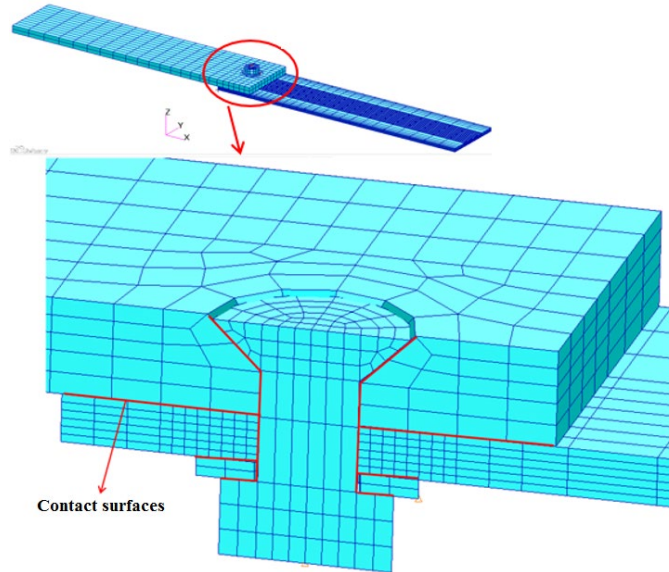

Figure 5. Contact elements in 3D model, contact surfaces marled with red colour

Another step in defining nonlinear contact phenomena is the choice between the analytical contact and the discreet contact, which will be briefly described below. When a node on a solid reaches the contact segment on the other contact body, the node is constraint on this segment with respect to the normal of this segment. In the case of discrete contact for normal detection, the linear representation with the finite elements of the contact surface is used, which leads to the calculation of the normal of each element.

If the surface is not planar, then when a node touches the contact segment, it is blocked between two different normal elements due to the discontinuity of the normal elements, because it is shifted and constrained on the contact segment. This impediment has an adverse effect on the quality of the results as observed by McCarthy et al., [35], in their work on composite bolted joints.

In the case of analytical contact, a smooth Coons surface is constructed through the nodes of the solid contact segment, and then this analytical surface is used to calculate the normal of the contact surface between the two solids, thus solving the problem of node blocking due to the discontinuity of the surface normal between the bodies. This method leads to a better representation of the geometry of the joint, especially its deformation and the accuracy of the numerical results is far superior to the technique of discrete contact, [35].

Table 3. FEM description

Part	Elements	Nodes
Composite adherent	3568	3284
Metal adherent	2413	2318
Bolt	862	824
Washer	394	357
All	7237	6783

3. TEMPERATURE EFFECTS ON THE JOINT STIFFNESS

- Model validation

In this section, the results from the tests are compared to the ones of the three-dimensional finite element model described in the previous chapter. Strains at the selected points on the surface of the laminated adherent are used to check the accuracy of the finite element model. The joints were strain gauged and loaded in tension to a level that prevents any damage of the composite adherent (1.2 kN load) at $T_1 = +50$ ºC.

Fig. 6 presents the locations of the 3 mm length strain gauges, type 1-Ly16-3/350, with 350 Ω electrical resistance, fabricated by HBM; gauges 1, 3, and 4 are aligned with the loading direction and located on the bottom surface of the laminate adherent, except the gauge number 2 which is located in the shear plane on the top surface of the composite adherent.

The numerically calculated and experimentally measured strains are given in Table 4 and Fig. 7. In Fig. 7 EXP curves denote the experimental strains, and FEM, the numerical ones.

From Table 4 it is clearly seen that strain gauges 1 and 2 indicate a joint bending, despite the fact that the loading is a tensile one. The strain readings for gauges 3 and 4 are quite different, thus indicating a twisting effect of the joint along the longitudinal axis, which is the loading x axis.

As a conclusion, from Table 4, it can be considered that the model has predicted the linear behavior of the joint quite satisfactory and can be further used in the following temperature parametric study for the linear response of the hybrid metal-composite joint.
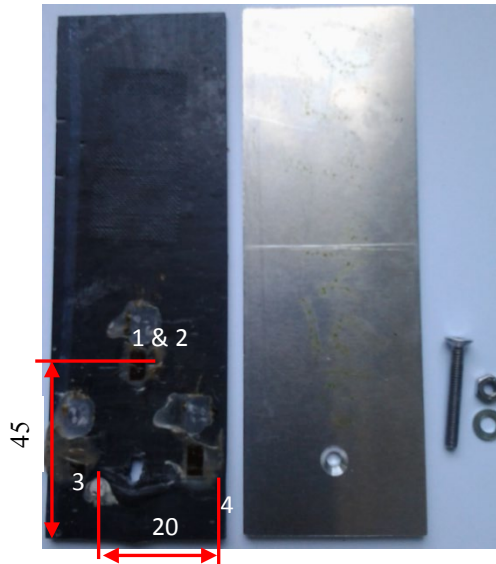

Figure 6. Strain gauge locations, all dimensions in mm

Table 4. Experimental and numerical strain readings, 1.2 kN applied load

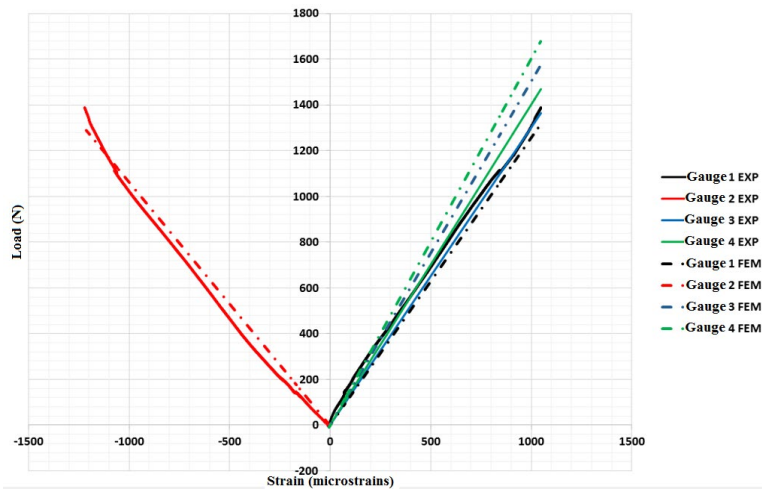| Gauge number	Experimental strain (μm/m)	Numerical strain (μm/m)
1	776	810
2	-1300	-1252
3	757	689
4	679	615

Figure 7. Experimental and numerical surface strains

- Joint stiffness

The effects of temperature on the joint axial stiffness are presented in this subchapter. From the experimental results, it was observed in Fig. 8 that the load-displacement curves are approximately linear, for applied load between 0.2 - 1 kN in the experiment and 0.1-1.5 kN in the simulation for the temperature T_1 = +50 ^{0}C, but in between 0.1-3.3 kN in experimental testing and 0.2-3.5 kN in FEA for the temperature T_2 = - 50 ^{0}C; so the stiffness of the joint is determined for these load ranges.

The joint load was directly obtained from the testing machine and the displacement was measured with an optical extensometer (Instron Advanced Video Extensometer). The load-displacement curves for the four temperature values are presented in Fig. 8.
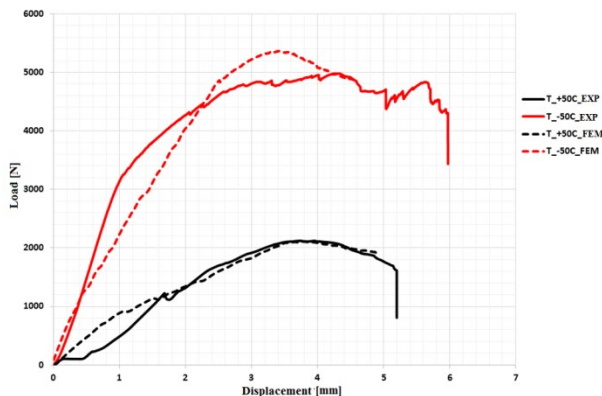

Figure 8. Load-displacements characteristic curves

The first nonlinear segments on the experimental curves from Fig. 8 are explained by the friction between the adherents.

For the low level of the applied load, the forces are transmitted through friction between the adherents without relative movement, so the shank of the bolt does not bear the hole surface due to the initial clearance in the joint.

The joint under investigation has a close tolerance clearance equal to 48 μm according to f7H10, [36], standard fit tolerances.

As long as F > μP, where F is the applied load, μ=0.235 is chosen to be the frictional coefficient between aluminum AA 7075 and CFRP adherents, as Schon [37] measured experimentally, and P = 330 N is the adherents clamping force due to bolt torque; the friction is overcome and the bolt shank moves toward the hole surface, reducing the joint clearance. Once the bolt fully contacts the hole surface, the joint is elastically deformed, the joint axial stiffness is developed and can be determined. The experimental and numerical axial stiffness, calculated as the slope of the approximately linear portions of the load-displacement curves in the load ranges mentioned above, are presented in Table 5 and Fig. 8. From Table 5 and Fig. 8, it can be observed that the temperature increase reduces the stiffness of the hybrid metal-composite joint both in the experiment and simulation, due to the fact that the matrix has plastic strains under high temperature and due to the low volume ratio of carbon within the composite material (32 %).

Table 5. Thermal effects on axial stiffness

Stiffness (kN/mm)		Temperature(^{0}C)
Experiment	Simulation	
3.49	1.83	-50
1.04	1.66	+50

4. CONCLUSIONS

In this paper, the thermal effects on the stiffness, damage initiation and progressive failure for single-lap, single-bolt, hybrid metal-composite joints are investigated using both experimental technique and finite element analysis (FEA). The joint geometry dimensions are designed according to ASTM D 5961 [26] standard for bearing failure. The tests were conducted using a universal testing machine, Instron 3367 connected to a controlled temperature chamber. A 3D FEM model, which incorporates geometrical and friction contact full nonlinearities was developed in Patran commercial software for prediction of the joint stiffness.

The simulation results were in good agreement with the experiments in terms of load-displacement behavior, surface strains, joint stiffness, which denoted that the 3D FEM model including full nonlinearities and explicit solver are quite accurate and can predict the metal-composite joint mechanical behavior on both linear-elastic and nonlinear elastic ranges.

Regarding the thermal effects on the joint stiffness it can be seen from Table 5 that temperature decreases stiffness of the joint in the axial direction. The loading joint behavior released some interesting features at the beginning stage due to the friction between the adherents.

ACKNOWLEDGEMENTS

REFERENCES

[1] Y. Xiao and T. Ishikawa, Bearing strength and failure behavior of bolted composite joints, part II: modeling and simulation, *Compos Sci Tech*, **65**(7-8): 1032–1043, 2005.
[2] J. L. Chaboche, Continuum damage mechanics: part II – damage growth, crack initiation and crack Growth, *J of Appl Mech*, **55**(1): 59–72, 1988.

[3] F. K. Chang and K. Y., Chang Post-failure analysis of bolted composite joints in tension or shear-out mode failure, *J of Compos Mat*, **21**(9): 809–33,1987.

[4] L. B. Lessard and M. M. Shokrieh, Two-dimensional modeling of composite pinned-joint failure, *J of Compos Mat*, **29**(5):671–97, 1995.

[5] C. L. Hung and F. K. Chang, Bearing failure of bolted composite joints. Part II: model and verification, *J of Compos Mat*, **30**(12): 1359–400, 1996.

[6] S. J. Kim, J. S. Hwang and J. H. Kim, Progressive failure analysis of pin-loaded laminated composites using penalty finite element method, *AIAA J*, **36**(1): 75–80, 1998.

[7] P. P. Camanho and F. L. Matthews, A progressive damage model for mechanically fastened joints in composite laminates. *J of Compos Mat*, **33**(24): 2248–80, 1999.

[8] B. Okutan, The effects of geometric parameters on the failure strength for pin-loaded multi-directional fiber-glass reinforced epoxy laminate, *Compos Part B- Eng*, **33**(8): 567–8, 2002.

[9] K. I. Tserpes, G. Labeas, P. Papanikos, et al. Th. Kermanidis, Strength prediction of bolted joints in graphite/epoxy composite laminates. *Compos Part B- Eng* 2002; **33**(7): 521–9.

[10] Olmedo Á and Santiuste C. On the prediction of bolted single-lap composite joints. *Compos Struct* 2012; **94**(6): 2110–7.

[11] Z. Kapidzˇic´, L. Nilsson and H. Ansell, Finite element modeling of mechanically fastened composite-aluminum joints in aircraft structures, *Compos Struct* 2014; **109**(6): 198–210.

[12] A. K. Zerbst, G. Kuhlmann and C. Steenbock, Progressive damage analysis of composite bolted joints with liquid shim layers using constant and continuous degradation models, *Compos Struct* 2010; **92**(2): 189–200.

[13] G. Kolks and K. I. Tserpes, Efficient progressive damage modeling of hybrid composite /titanium bolted joints, *Compos Part A- Appl S and Manuf* 2014; **56**(1): 51–63.

[14] B. Egan, M. A. McCarthy, R. M. Frizzell, et al., Modelling bearing failure in countersunk composite joints under quasi-static loading using 3D explicit finite element analysis, *Compos Struct* 2014; **108**: 963–977.

[15] A. Olmedo, C. Santiuste and E. Barbero, An analytical model for the secondary bending prediction in single-lap composite bolted-joints, *Compos Struct* 2014; **111**: 354–361.

[16] H. da Costa Mattos, J. Reis, L. Paim, et al., Analysis of a glass fibre reinforced polyurethane composite repair system for corroded pipelines at elevated temperatures, *Compos Struct* 2014; **114**:117–23.

[17] J. Reis, J. Coelho, A. Monteiro and da H. Costa Mattos, Tensile behavior of glass/epoxy laminates at varying strain rates and temperatures, *Compos Part B- Eng* 2012; **43**(4): 2041–2046.

[18] Reis J, Coelho J and da Costa Mattos H. A continuum damage model for glass/epoxy laminates in tension. *Compos Part B- Eng* 2013; 52: 114–9.

[19] J. Reis, F. Amorim, A. da Silva, et al., Influence of temperature on the behavior of DGEBA (bisphenol A diglycidyl ether) epoxy adhesive, *Int J of Adhes and Adhes* 2015; **58**: 88–92.

[20] J. Zhengwen, W. Shui and W. Zhishen, Calculation of energy release rate for adhesive composite/metal joints under mode-I loading considering effect of the non-uniformity, *Compos Part B- Eng* 2016; **95**:374–85.

[21] M. Heshmati, R. Haghani and M. Al-Emrani, Durability of bonded FRP-to-steel joints: effects of moisture, de-icing salt solution, temperature and FRP type, *Compos Part B- Eng* 2017; **119**: 153–167.

[22] T. Kleffel and D. Drummer, Investigating the suitability of roughness parameters to assess the bond strength of polymer-metal hybrid structures with mechanical adhesion, *Compos Part B- Eng* 2017; **117**: 20–5.

[23] A. Agarwal, S. Foster and E. Hamed, Wet thermo-mechanical behavior of steel–CFRP joints – an experimental study, *Compos Part B- Eng* 2015; **83**: 284–296.

[24] A. Agarwal, S. Foster, E. Hamed, et al., Testing of steel-CFRP adhesive joints under freeze-thaw cycling, In: *Conf. Mech. Struct. Mater. ACMSM 2012*, pp. 801–6.

[25] M. Heshmati, R. Haghani and M. Al-Emrani, Effects of moisture on the long-term performance of adhesively bonded FRP/steel joints used in bridges, *Compos Part B- Eng* 2016; **92**: 1–16.

[26] * * * ASTM D 5961:2007, *Standard test method for bearing response of polymer matrix composite laminates*.

[27] M. Chishti, H. Wang, S. Thomson, et al., Experimental investigation of damage progression and strength of countersunk composite joints, *Compos Struct* 2012; **94**(3): 865–873.

[28] * * * ASTM D 3039: 2002, *Standard Test Method for Tensile Properties of Polymer Matrix Composite Materials*.

[29] * * * ASTM D 3410: 2007, *Standard Test Method for Compressive Properties of Polymer Matrix Composite Materials*.

[30] * * * ASTM D 5379:2008, *Standard Test Method for Shear Propeties of Composite Materials by the V-Notched Beam Method*.

[31] * * * Toray Carbon Fibers America Inc., *Torayca T300, Technical Data Sheet*, Report no. CFA-001, 2010, USA.

[32] * * * Ashland Inc., *Derakane Momentum 411-350 Epoxy Venyl Ester Resin*, Technical Data Sheet No. 1701 V3 F2, 2010, USA.

[33] * * * ESA ESTEC, *Design calculation methods and general design aspects*, Structural materials handbook, ECSS-E-HB-32-20 Part 2A, 2011.

[34] * * * Federal Aviation Administration, *Metallic Materials Properties development and Standardization*, 2010, USA.

[35] M. A. McCarthy, C. T. McCarthy, V. P. Lawlor, et al., Three-dimensional finite element analysis of single-bolt, single-lap composite bolted joints: part I - model development and validation, *Compos Struct* 2005; **71**: 140–158.

[36] * * * ISO 286-2:2010, *Tables of standard tolerance classes and limit deviations for holes and shafts*.

[37] J. Schon, Coefficient of friction for aluminum in contact with a carbon fiber epoxy composite, *Trib Int* 2004; **37**(5): 395–404.

[38] H. Hahn and S. Tsai, Nonlinear elastic behavior of unidirectional composite laminates, *J of Compos Mater* 1973; **7**(1):102–18.

[39] D. Ao, L. Yuqing, X. Haohui, et al., Progressive damage analysis of PFRP double-lap bolted joints using explicit finite element method, *Compos Struct* 2016*,* **152**: 860–869.

[40] Z. Hashin, Failure criteria for unidirectional fiber composites, *J of Appl Mech* 1980; **47**(2): 329–34.

[41] Y. Zhou, H. Yazdani-Nezhad, M. Mccarthy, et al., A study of intra-laminar damage in double-lap, multi-bolt, composite joints with variable clearance using continuum damage mechanics, *Compos Struct* 2014, **116**(9): 441–452.

[42] R. O'Higgins, *An experimental and numerical study of damage initiation and growth in high strength glass and carbon fibre-reinforced composite materials*, PhD Thesis, University of Limerick, Ireland, 2007.

[43] P. P. Camanho and M. Lambert, A design methodology for mechanically fastened joints in laminate composite materials. *Compos Sci and Tech* 2006, **66**: 3004-3020.

[44] M. R. Garnich and M. K. Akula, Review of degradation models for progressive failure analysis of fiber reinforced polymer composites, *ASME* 2009, **62**: 1-33.